Developmental waves in myxobacteria: A distinctive pattern formation mechanism

Oleg A. Igoshin
Department of Physics, University of California, Berkeley, California 94720, USA

John Neu
Department of Mathematics, University of California, Berkeley, California 94720, USA

George Oster*
Departments of Molecular and Cellular Biology and of Environmental Science, Policy and Management, University of California, Berkeley, California 94720, USA

(Received 31 May 2004; published 29 October 2004)

In early stages of their development, starving myxobacteria organize their motion to produce a periodic pattern of traveling cell density waves. These waves arise from coordination of individual cell reversals by contact signaling when they collide. Unlike waves generated by reaction-diffusion instabilities, which annihilate on collision, myxobacteria waves appear to pass through one another unaffected. Here we analyze a mathematical model of these waves developed earlier [Igoshin *et al.*, Proc. Natl. Acad. Sci. USA **98**, 14 913 (2001)]. The mechanisms which generate and maintain the density waves are clearly revealed by tracing the reversal loci of individual cells. An evolution equation of reversal point density is derived in the weak-signaling limit. Linear stability analysis determines parameters favorable for the development of the waves. Numerical solutions demonstrate the stability of the fully developed nonlinear waves.

DOI: 10.1103/PhysRevE.70.041911 PACS number(s): 87.18.Hf, 87.18.Ed, 87.18.La

I. INTRODUCTION

Waves and wavelike phenomena are everywhere in nature but their underlying mechanisms are very diverse. Well-studied examples include inertial waves in fluid mechanics and elasticity and Turing instability waves in excitable chemical media. The latter mechanism has been used to model a variety of biophysical phenomena such as calcium waves in vertebrate eggs[1], progression of epidemic fronts [2], chemotactic waves of the slime mold *Dictyostelium discoideum* [3–6], and pigmentation patterns on sea shells [7,8] and other animals [9,10] (see also [2] and references therein). The Turing mechanism depends crucially on diffusion and so these patterns are referred to as diffusion-reaction patterns. In contrast, the density waves observed during the development of *Myxococcus xanthus* arise in a completely different way.

Myxobacteria are rod-shaped bacteria, well known for their social lifestyle and complex developmental patterns [11–18]. Under starvation conditions cells aggregate into multicellular mounds called fruiting bodies. Just before the aggregation begins the surface of the colony is often covered with well-organized periodic patterns of equispaced high-cell-density bands that move as traveling waves, often referred to as "ripples" (Fig. 1) [14,15,18]. In certain circumstances the waves can persist for hours with no net mass transport [14], analogous to water waves. The wave crests *appear* to pass through one another with no interference [14]. Actually, the waves do not interpenetrate, but reflect off one another when they collide. We have come to refer to them as "accordion waves," and they are quite unlike the chemotactic waves in *Dictyostelium discoideum* [3–6] or chemical waves [2,19] that annihilate on collision. *Dictyostelium* waves are based on induced release of an attractant, cAMP, by each cell to which they respond by moving up the local cAMP gradient. The pattern formation mechanism in

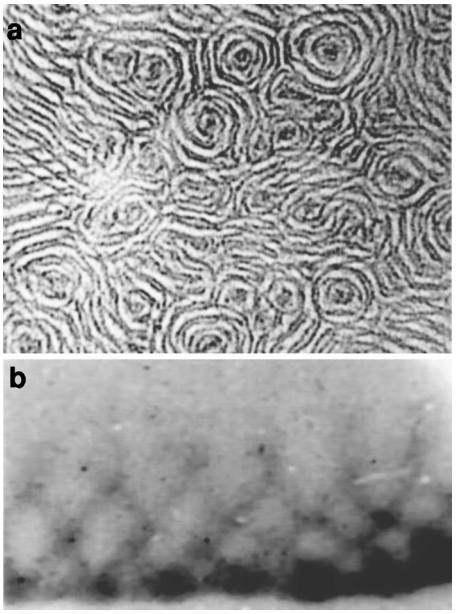

FIG. 1. Ripples as seen in phase contrast microscopy. (a) Coexisting planar, spiral, and concentric waves (courtesy of Brian Sager and Dale Kaiser). (b) Planar waves at the edge of submerged culture (courtesy of Roy Welch and Dale Kaiser).

*Corresponding author. FAX: (510) 642-7428. Electronic address: goster@nature.berkeley.edu

myxobacteria is different because they communicate only by direct cell contact [20,21].

II. MATHEMATICAL MODEL

The mathematical model describing the ripple phase was presented in Ref. [22] based on experimental observations summarized in Refs. [14,15]. The essential ingredients of the model are as follows.

(i) Each myxobacterium glides along its long axis. It periodically reverses its gliding direction not by making a U turn, but by switching its "front" and "rear" ends. An internal biochemical cycle controls the reversals in direction.

(ii) Cells collide with oppositely moving cells. During each "head-to-head" collision cells exchange a contact signal which accelerates their reversal cycle. The collision frequency—and therefore the signaling intensity—is proportional to the local cell density.

(iii) After each reversal the cell enters a "refractory period" during which it does not respond to collision signaling and does not reverse.

In many experimentally observed situations rippling is essentially a one-dimensional phenomenon since cells are predominantly aligned in parallel. For instance, in Ref. [15] cells glide parallel to an impermeable boundary of a submerged culture [Fig. 1(b)]. In different conditions [Fig. 1(a)] myxobacteria generate complex patterns of interpenetrating planar, spiral, and concentric waves [14]. These wave patterns can be reproduced by the mathematical model summarized above if the cell orientation dynamics is taken into account [23]. In this paper we will restrict ourselves to one-dimensional ripple patterns by assuming that cells only move parallel to the x axis.

In order to represent the internal biochemical cycle mathematically we map it onto the circle as shown in Fig. 2(a) and describe it by a phase coordinate ϕ. Cells with $0<\phi<\pi$ move to the right ($+x$ direction), and cells with $\pi<\phi<2\pi$ move to the left ($-x$). Therefore, a population of cells can be characterized by the density function $n(x,\phi,t)$ giving the number of cells in a neighborhood of point x with phase ϕ at time t. Since cell division and death are negligible on the time scale of rippling, the density obeys the conservation equations

$$\partial_t n + v_0\partial_x n + D_x\partial_{xx}n + \partial_\phi(\omega_+ n) + D_\phi\partial_{\phi\phi}n = 0 \text{ in } 0<\phi<\pi, \tag{1}$$

$$\partial_t n - v_0\partial_x n + D_x\partial_{xx}n + \partial_\phi(\omega_- n) + D_\phi\partial_{\phi\phi}n = 0 \text{ in } \pi<\phi<2\pi. \tag{2}$$

Here $v_0=$const is the spatial velocity of individual cells; $\omega_+(x,\phi,t)$ and $\omega_-(x,\phi,t)$ are the angular (phase) velocities describing how fast cells at a given position and phase progress through their reversal cycle. The diffusion terms in Eqs. (1) and (2) model random fluctuations in space and phase velocities.

Right after reversals, in phase intervals $0<\phi<\alpha$ and $\pi<\phi<\pi+\alpha$ the cells do not respond to signaling and progress with constant angular speed ω_0 [Fig. 2(a)] :

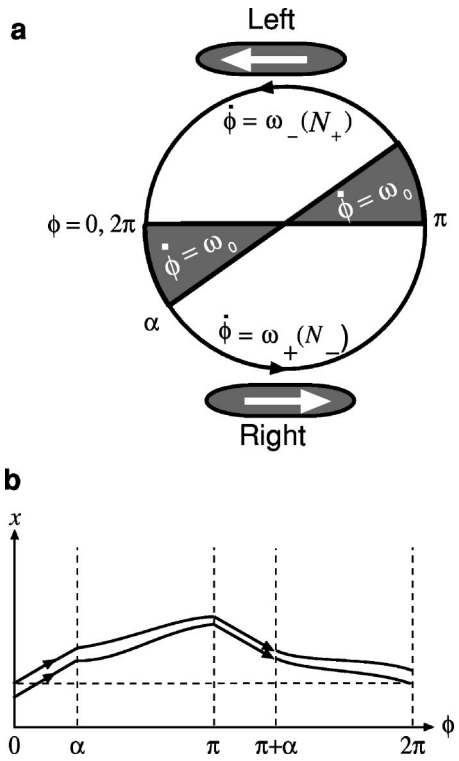

FIG. 2. (a) Mapping of the internal biochemical cycle on a circle. (b) Typical cell trajectories on the (x,ϕ) plane. Arrows show the direction of increasing time.

$$\omega_+(x,0<\phi<\alpha,t) = \omega_-(x,\pi<\phi<\pi+\alpha,t) = \omega_0.$$

In the sensitive intervals of their cycles ($\alpha<\phi<\pi$, $\pi+\alpha<\phi<2\pi$), the cell phase velocity is determined by the number of collisions (signaling events) they receive. We shall assume that most of the collisions occur between oppositely moving cells with a rate proportional to the local cell density. Therefore,

$$\omega_+(x,\alpha<\phi<\pi,t) = \omega(N_-(x,t)),$$

$$\omega_-(x,\pi+\alpha<\phi<2\pi,t) = \omega(N_+(x,t)),$$

where

$$N_+(x,t) = \int_0^\pi n(x,\phi,t)d\phi, \quad N_-(x,t) = \int_\pi^{2\pi} n(x,\phi,t)d\phi \tag{3}$$

are the local densities of right and left going cells at a given point x, regardless of phase. The function ω determines density dependence of signaling. We chose ω to be a generic saturating sigmoid function [22]

$$\omega(N) = \omega_0 + \omega_1 \frac{N^q}{N^q + N_{cr}^q}. \tag{4}$$

Here $\omega(0)$ can be chosen to be equal to the phase velocity in the refractory period.[1]

One can track paths of individual cells in the (x,ϕ) plane. Figure 2(b) represents typical trajectories of a cell in the absence of diffusion. In the first refractory phase interval $(0,\alpha)$ a cell moves at constant speed $+v_0$ in the x direction and constant speed ω_0 in the ϕ direction, and so the cell trajectory is represented by a straight line. As a cell enters its first sensitive period it continues to glide with speed $+v_0$ in the x direction but speeds up in ϕ depending on the local density of counterpropagating cells according to Eq. (4). Hence, the cell's trajectory curves downward in this interval. At phase $\phi=\pi$, the cell reverses its spatial direction. The spatial and phase velocities in the second refractory interval $\pi<\phi<\pi+\alpha$ are $-v_0$ and ω_0, respectively. In the second sensitive interval the cell accelerates in the ϕ direction and its trajectory curves upward. When the cell reaches $\phi=2\pi$, it continues, starting with $\phi=0$ and the same x.

Numerical solutions of the model equations show that, over a certain range of parameters, spatially homogeneous solutions are unstable [22]. Depending on the boundary conditions it is possible to produce either unidirectional or counterpropagating waves as steady-state solutions [22,23]. Semiquantitative arguments show that the wavelength λ is given by [22]

$$\lambda \approx 2v_0\tau_R, \tag{5}$$

where τ_R is the average time between reversals.

The outline of the subsequent parts of the paper is as follows. In the next section we show that the mechanisms which generate and maintain the density waves are clearly revealed by tracing the reversal points of individual cells. An evolution equation of reversal point density is derived in the weak-signaling limit. In the body of the paper we present a geometric derivation of the evolution equation. A more formal derivation based on asymptotic expansions is presented in the Appendix. Section IV analyzes unidirectional-wave solutions with speed near v_0. The linear stability analysis of the evolution equation determines the range of model parameters for the growth of waves with wavelength given by Eq. (5) and with speed near v_0. A more general linear instability analysis is performed in Sec. V. The results of this section indicate that the linear stability analysis of the weak-signaling model does not provide a wave speed and wavelength selection mechanism. Numerical simulations and analysis performed in Sec. VI demonstrate the stability and focusing mechanism of the fully developed nonlinear waves.

[1]Let ϕ be an assignment of phase so that the refractory phase velocity is $\dot{\phi}=w_0$ for $0<\phi<\alpha$. Define a new phase ψ, related to ϕ by a "gauge transformation" $\psi(\phi)$. Then the angular velocity with respect to ψ in the refractory period is $\omega=\dot{\psi}=\psi'(\phi)\omega_0$. We can always enforce $\omega=\omega(0)$ in $0<\psi<\psi(\alpha)$ by choosing $\psi'(\phi)=\omega(0)/\omega_0$.

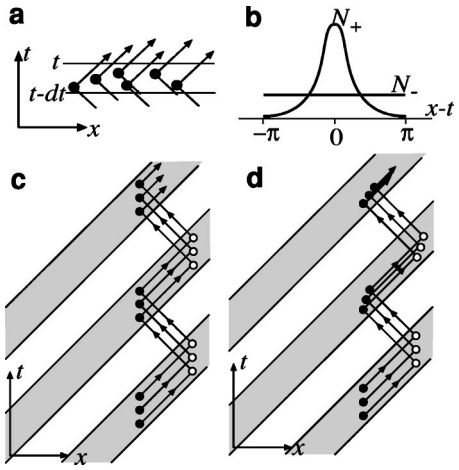

FIG. 3. (a) Reversal points in the interval $(t-dt,t)$: cells that reverse from left to right in the time interval $(t-dt,t)$ would have phases $(0,dt)$ at time t. (b) Example of a kinematic right-traveling wave solution. (c) Space-time trajectories of cells in the kinematic right-traveling wave. (d) The same as in (c) but perturbed by weak signaling. Cells entering the crest reverse faster and are focused: i.e., the cell density increased with each reversal.

III. REVERSAL-POINT DENSITY

Before we proceed with the analysis it is convenient to nondimensionalize Eqs. (1) and (2) so that

$$\omega_0 = 1, \quad v_0 = 1, \quad N_{cr} = 1. \tag{6}$$

Therefore, we measure time in units of $1/\omega_0$ and length in units of v_0/ω_0.

A. Kinematic waves

We begin by analyzing solutions of Eqs. (1) and (2) in the absence of signaling [$\omega_1=0$ in Eq. (4)] and diffusion ($D_\phi=D_x=0$). In this case Eqs. (1) and (2) reduce to

$$\partial_t n + \partial_x n + \partial_\phi n = 0, \quad \text{in} \quad 0<\phi<\pi, \tag{7}$$

$$\partial_t n - \partial_x n + \partial_\phi n = 0, \quad \text{in} \quad \pi<\phi<2\pi, \tag{8}$$

with n continuous across $\phi=\pi$ and $\phi=0(2\pi)$. The general solution of this boundary value problem is

$$n = \begin{cases} f(x-\phi,t-\phi), & 0<\phi<\pi, \\ f(x+\phi-2\pi,t-\phi), & \pi<\phi<2\pi, \end{cases} \tag{9}$$

where f is an arbitrary function, 2π periodic in its second argument:

$$f(x,t) = f(x,t-2\pi). \tag{10}$$

This property follows from continuity across $\phi=0(2\pi)$.

The function $f(x,t)$ has a clear physical interpretation. Consider the density of cells at point x that reverse from left to right between $t-dt$ and t [see Fig. 3(a)]. These cells have phases $0\leqslant\phi\leqslant dt$, so their density is $n(x,0,t)dt=f(x,t)dt$. Therefore, $f(x,t)$ represents the density of left-to-right (LR) reversal points in spacetime. By analogy, the density of right-

to-left (RL) reversal points is given by $f(x-\pi,t-\pi)$. Thus, in the absence of signaling and diffusion, Eqs. (7) and (8) allow us to recover the space-phase density distribution from the space-time density of reversal points. In addition, the spatial densities of right- and left-moving particles are given by

$$N_+(x,t) = \int_0^\pi f(x-\phi,t-\phi)d\phi, \tag{11}$$

$$N_-(x,t) = \int_\pi^{2\pi} f(x+\phi-2\pi,t-\phi)d\phi. \tag{12}$$

It is easy to show that, in the absence of signaling, Eqs. (7) and (8) admit kinematic traveling-wave solutions with speed ±1. Traveling waves of velocity +1 are obtained by taking $f(x,t)=F(t-x)$. It follows from Eq. (10) that F has to be 2π periodic. From Eq. (11) one concludes that

$$N_+(x,t) = \pi F(t-x). \tag{13}$$

From Eq. (12) it follows that

$$N_-(x,t) = \int_\pi^{2\pi} F(2(\pi-t-2\phi)-x)d\phi$$

$$= \frac{1}{2}\int_0^{2\pi} F(t+s-x)ds = \langle N_+\rangle. \tag{14}$$

Since $F(x)$ is 2π periodic, $N_-(x,t)$ is constant. The second equality shows that this constant is in fact the average value of $N_+(x,t)$ [Eq. (11)] over one period. Suppose that initially N_+ is a 2π-periodic sequence of narrow pulses and N_- is a constant equal to the average value of $\langle N_+\rangle$ [Fig. 3(b)]. The corresponding space-time trajectories of particles are shown in Fig. 3(b). Each of the particles travels in "zigzag" fashion on the (x,t) plane. The time duration between reversals is equal to π, the distance traveled between two consecutive reversals is also π, and the net displacement after two reversals is zero.

We now examine how signaling (even if very weak) perturbs this simple kinematics to induce focusing of the bands in Fig. 3(c) which counteracts diffusion. Figure 3(d) illustrates the focusing effect. As the left-going cells enter a band of right-going cells (i.e., a wave crest) they receive sufficient signals to reverse earlier than they otherwise would have. Consequently, the reversal points of these cells will drift closer together, sharpening the crest. This focusing effect will be counteracted by spreading due to fluctuations in speed and phase velocity, which we model as diffusion. In the following subsections we derive an equation describing how the evolution of the reversal point density is influenced by these effects.

B. Small-signaling limit

Figure 4 illustrates how signaling perturbs the mapping from one reversal point to the next. If (x,t) is a LR reversal point of a cell, then $(x,t+2\pi)$ is its next LR reversal point in the absence of signaling. In the presence of signaling this

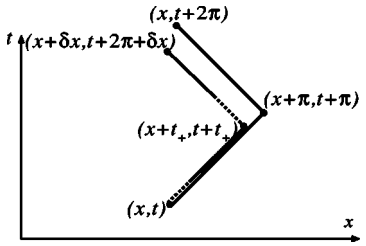

FIG. 4. Perturbations in a single-cell trajectory by a small signaling.

reversal point is perturbed by the vector $(\delta x,\delta t)$. Knowing the times t_+ and t_- that a cell travels to the right and left the components of the perturbation vector are [recalling Eq. (6)]

$$\delta x = t_+ - t_-, \quad \delta t = t_+ + t_- - 2\pi. \tag{15}$$

Assuming that the densities $N_\pm$ are given along the cell's trajectory, one can compute $\omega_\pm$ and obtain implicit equations for $t_\pm$. For instance, the phase shift between LR reversal at (x,t) and RL reversal at $(x+t_+,t+t_+)$ is given by

$$\pi = \int_0^{t_+} \omega_+(x+s,s,t+s)ds. \tag{16}$$

In the same fashion one obtains the opposite reversal phase shift by

$$\pi = \int_0^{t_-} \omega_-(x-s+t_+,\pi+s,t+s)ds. \tag{17}$$

Now consider the weak-signaling limit defined by

$$\omega(N) \equiv 1 + \epsilon\Omega(N), \tag{18}$$

where $\epsilon>0$ is a small gauge parameter. In this case Eqs. (16) and (17) can be solved iteratively for $t_\pm$. Substituting results into Eq. (15) one obtains

$$\delta x = \epsilon U(x,t) + O(\epsilon^2), \tag{19}$$

where

$$U \equiv \int_\alpha^\pi [\Omega(N_+(x+\pi-s,t+\pi+s)) - \Omega(N_-(x+s,t+s))]ds \tag{20}$$

and

$$\delta t = \epsilon V(x,t) + O(\epsilon^2), \tag{21}$$

where

$$V \equiv -\int_\alpha^\pi [\Omega(N_+(x+\pi-s,t+\pi+s)) + \Omega(N_-(x+s,t+s))]ds. \tag{22}$$

Note that in order to obtain the leading $O(\epsilon)$ terms in the expansion for U and V one can use expressions for $N_\pm$ in the no-signaling limit—i.e., Eqs. (11) and (12). Consequently,

$$U \sim \int_{\alpha}^{\pi} ds \left[\Omega\left(\int_0^{\pi} f(x-s+\phi, t+s+\phi) d\phi \right) - \Omega\left(\int_0^{\pi} f(x+s-\phi, t+s+\phi) d\phi \right) \right] \tag{23}$$

and

$$V \sim -\int_{\alpha}^{\pi} ds \left[\Omega\left(\int_0^{\pi} f(x-s+\phi, t+s+\phi) d\phi \right) + \Omega\left(\int_0^{\pi} f(x+s-\phi, t+s+\phi) d\phi \right) \right]. \tag{24}$$

These results enable us to construct a mapping of the reversal-point distribution: Suppose one is given the reversal-point density distribution $f(x,t)$ for all x and $0 \leqslant t < 2\pi$. We can construct the mapping of this reversal-point distribution to the next time slice $2\pi \leqslant t < 4\pi$. The reversal point densities $f(x,t)$ and $f(x+\delta x, t+2\pi+\delta t)$ are related by the Jacobian describing changes in the space-time unit area:

$$f(x,t) = f(x+\delta x, t+2\pi+\delta t) \begin{vmatrix} 1+\partial_x(\delta x) & \partial_x(\delta t) \\ \partial_t(\delta x) & 1+\partial_t(\delta t) \end{vmatrix}. \tag{25}$$

Substituting Eqs. (19), (21), (23), and (24) into Eq. (25) and expanding f in a Taylor series, one obtains

$$f(x,t+2\pi) - f(x,t) + \epsilon\{\partial_x(Uf) + \partial_t(Vf)\} = O(\epsilon^2). \tag{26}$$

Note that in order to determine U and V from Eqs. (23) and (24) one has to use values of f from 0 to 4π—i.e., from both time slices. Therefore, the mapping (26) looks implicit. However, since U and V appear only in $O(\epsilon)$ perturbation terms, one can use a periodic extension of f into the $2\pi < \phi < 4\pi$ time slice to make this mapping explicit. Defining

$$f_n(x,t) = f(x, t+2\pi n), \quad 0 \leqslant t < 2\pi, \tag{27}$$

one can generalize Eq. (26) as

$$f_{n+1}(x,t) - f_n(x,t) + \epsilon\{\partial_x(U_n f_n) + \partial_t(V_n f_n)\} = O(\epsilon^2). \tag{28}$$

The subindex n on U and V implies that they are evaluated using f_n and its periodic extension.

In the limit of small ϵ but large $n = O(1/\epsilon)$ one can asymptotically rewrite this iteration mapping as a partial differential equation (PDE) for $f(x,t,T \equiv \epsilon n)$:

$$\partial_T f + \partial_x(Uf) + \partial_t(Vf) = 0. \tag{29}$$

C. Effects of fluctuations on the phase velocity and speed

Fluctuations in the spatial and phase velocities of individual cells are inevitable. We model them by adding independent random terms $r_x(t)$ and $r_\phi(t)$ to the spatial and phase velocities, respectively:

$$\frac{d\phi}{dt} = \omega_{\pm} + r_\phi(t), \quad \frac{dx}{dt} = 1 + r_x(t). \tag{30}$$

If one assumes "white noise" specta for the fluctuations r_ϕ and r_x,

$$\langle r_\phi \rangle = \langle r_x \rangle = 0, \quad \langle r_\phi(t) r_\phi(0) \rangle = D_\phi \delta(t), \tag{31}$$

$$\langle r_x(t) r_x(0) \rangle = D_x \delta(t),$$

then the noise terms manifest themselves as diffusion terms in Eqs. (1) and (2) for densities. In this subsection we derive how diffusion affects the evolution of the reversal-point density f. In general, for steady wave solutions to exist the diffusion terms must have the same scaling as the signaling—i.e.,

$$D_x \equiv \epsilon D_1, \quad D_\phi \equiv \epsilon D_2. \tag{32}$$

The effects of diffusion and signaling can be shown to be additive to leading order in ϵ. We will assume this additivity and derive the evolution of the reversal-point density with noise but zero signaling.

Integrating the phase equation (30) one obtains equations for t_+, the duration of the right-going interval

$$\pi = t_+ + \int_0^{t_+} r_\phi(s) ds.$$

Using Eq. (31) and (32) one obtains

$$\langle t_+ \rangle = \pi, \quad \langle (t_+ - \pi)^2 \rangle = 2\pi\epsilon D_2. \tag{33}$$

The same formulas hold for t_-, the duration of the left-going interval. The time drift of the reversal points is given by

$$\delta t = t_+ + t_- - 2\pi = (t_+ - \pi) + (t_- - \pi).$$

Thus,

$$\langle (\delta t)^2 \rangle = 4\pi\epsilon D_2. \tag{34}$$

In the same fashion we obtain that

$$\delta x = (t_+ - \pi) - (t_- - \pi) + \int_0^{t_+ + t_-} r_x(s) ds,$$

$$\langle (\delta x)^2 \rangle = 4\pi\epsilon D_2 + 4\pi\epsilon D_1. \tag{35}$$

Therefore, noise terms result in diffusion in the reversal-point density equation with diffusion constant $2\pi D_2$ in t and $2\pi(D_1 + D_2)$ in x. The resulting equation for $f(x,t,T)$ is

$$\partial_T f + \partial_x(Uf) + \partial_t(Vf) = 2\pi(D_1 + D_2)\partial_{xx} f + 2\pi D_2 \partial_{tt} f. \tag{36}$$

In the Appendix we show an alternative way of deriving this equation based on multiple-scale asymptotic analysis.

In some range of parameters the focusing effects of the convective terms in Eq. (36) would dominate the diffusion terms so that the homogeneous solution becomes unstable. The easiest way to illustrate this is to consider unidirectional traveling waves.

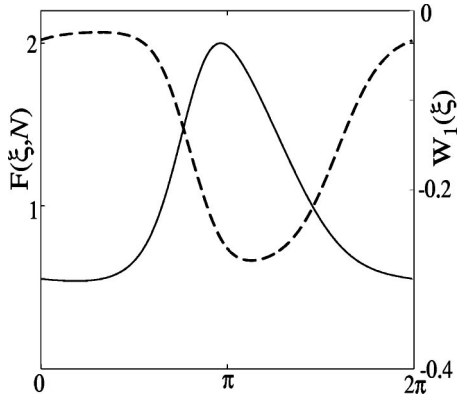

FIG. 5. Solution $F(\xi,T)$ of Eq. (38) for large T, left axis, solid line, and corresponding focusing velocity W_1 [see Eq. (40)], right axis, dashed line. The parameters used are as follows: $D_1+2D_2=0.1$, $\Omega(N)=N^4/(1+N^4)$, and $\alpha=0.15\pi$.

IV. UNIDIRECTIONAL WAVES OF SPEED 1

We have shown that, in the absence of signaling and diffusion, there are kinematic waves of speed 1. In the presence of weak signaling and small diffusion, Eq. (36) allows finite-stationary-amplitude traveling-wave solutions with speed near 1. We search for solutions of Eq. (36) of the form

$$f(x,t,T)=F(\xi,T), \quad \xi \equiv x-t. \tag{37}$$

It follows from Eq. (10) that F has to be 2π periodic. In dimensional units this period corresponds to the wavelength $\lambda=2v_0\tau_R$ in Eq. (5). $F(\xi,T)$ obeys

$$\partial_T F + 2\partial_\xi(WF) = 2\pi(D_1+2D_2)\partial_{\xi\xi}F, \tag{38}$$

where

$$\begin{aligned} W(\xi) &= U - V \\ &= 2\int_\alpha^\pi \Omega(\pi F(\xi-2s,T))ds \\ &= \int_{2\alpha}^{2\pi} \Omega(\pi F(\xi-\psi,T))d\psi. \end{aligned} \tag{39}$$

The last equality allows one to see that, if there is no refractory period ($\alpha=0$), then because F is periodic, the velocity W does not depend on ξ and so provides a constant drift rather than focusing. It is convenient to separate out this drift by rewriting Eq. (39) in the form

$$\begin{aligned} W(\xi) &= \int_0^{2\pi} \Omega(\pi F(\xi-\psi,T))d\psi - \int_0^{2\alpha} \Omega(\pi F(\xi-\psi,T))d\psi \\ &\equiv W_0 + W_1(\xi). \end{aligned} \tag{40}$$

Figure 5 shows typical solution of Eq. (38) and the corresponding drift velocity. As one can see from Fig. 5 and from Eq. (40), W_1 is always negative and its minimum is shifted to the right of maximum of F by 2α. Hence, cells at the front of the wave crest tend to drift toward the cells in the back of the crest—i.e., keeping the waves focused. This focusing balances diffusive spreading of the crest to create the finite-amplitude steady waves (Fig. 5).

Numerical simulations of Eq. (38) show that the wave amplitude decreases with increasing diffusion or decreasing signal strength. At some point spatially homogeneous solutions become stable solutions. To obtain an estimate of this threshold we perform a linear instability analysis of Eq. (38) about the homogeneous solution

$$\pi F(\xi,T) = N + G(\xi,T). \tag{41}$$

The linearized equation for $G(\xi,T)$ is

$$\partial_T G + 2W^{(0)}\partial_\xi G + 2N\partial_\xi W^{(1)} = 2\pi(D_1+2D_2)\partial_{\xi\xi}G, \tag{42}$$

where

$$W^{(0)} = 2\Omega(N)(\pi-\alpha),$$

$$\begin{aligned} \partial_\xi W^{(1)} &= \partial_\xi \int_{2\alpha}^{2\pi} \Omega'(N)G(\xi-\psi)d\psi \\ &= \Omega'(N)[G(\xi-2\alpha)-G(\xi)]. \end{aligned}$$

Equation (42) has exponential solutions of the form

$$G(\xi,T) \propto \exp(\sigma T + ik\xi), \tag{43}$$

where $k=1,2\ldots$; i.e., k is an integer to ensure 2π periodicity of solutions. Using Eq. (43) in Eq. (42) we obtain

$$\sigma = -4i\Omega(N)(\pi-\alpha) - 2N\Omega'(N)(e^{-2i\alpha k}-1) + 2\pi(D_1+2D_2)k^2. \tag{44}$$

The growth rate Γ is given by

$$\Gamma \equiv \mathrm{Re}(\sigma) = 2N\Omega'(N)[\sin^2(\alpha k) - Ck^2], \tag{45}$$

where the competition of diffusion and focusing is expressed by a parameter

$$C \equiv \pi(D_1+2D_2)/[N\Omega'(N)] = \pi(2D_\phi + D_x)/[N\omega'(N)]. \tag{46}$$

In the last last equality we expressed C in terms of the unscaled phase velocity and diffusion using Eqs. (18) and (32).

Figure 6 shows the neutral stability curves defined by $\Gamma=0$ for different wave numbers k. From Eq. (45) it follows that a given wave number will grow for parameter values below the corresponding curve. It is evident that the growth region for each wave number would include growth regions of all larger wave numbers as a subset. The shaded region of Fig. 6 depicts the region where only the $k=1$ wave grows. This wave number corresponds to the wavelength $\lambda=2v_0\tau_R$ [Eq. (5)]. Higher wave numbers correspond to smaller wavelengths. In the area above the solid line in Fig. 6 the growth rate is always negative $\Gamma<0$ so that the homogeneous state is stable. Thus unidirectional waves with speed near 1 grow if

$$\pi(2D_\phi + D_x) < [N\omega'(N)]\sin^2\alpha. \tag{47}$$

This criterion is similar to the one developed in Ref. [22] by semiquantitative arguments. Equation (47) refines that analy-

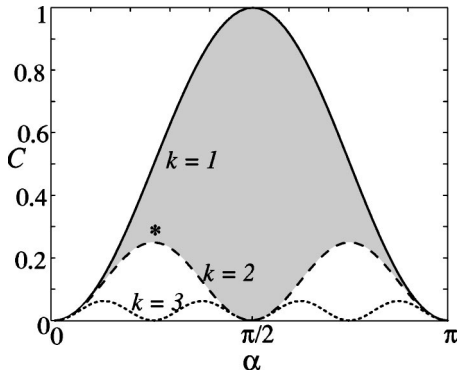

FIG. 6. Neutral stability curves for different wave numbers: $k=1$, solid line; $k=2$, dashed line; and $k=3$, dotted line. The shaded area shows the parameters where only one wavelength is growing.

sis in several important ways. It shows how space and phase diffusion contribute differently to the spreading of the waves [left-hand side of Eq. (47)]. It also shows how the focusing effects [right-hand side of Eq. (47)] depend on the duration of the refractory period α which was just assumed to be big enough in Ref. [22]. With the density dependence of $\omega(N)$ given by Eq. (4) the term in the square brackets in Eq. (47) is maximum at $N=N_{cr}$ and is proportional to the cooperativity of the signaling q. This agrees with the numerical results of Ref. [22].

If the refractory period α is sufficiently small, Fig. 6 shows that the interval of C corresponding to growth of $k=1$ waves only is also small. Simulation of the full set of equations (1)–(4) shows that, at sufficiently strong signaling, the right wavelength is selected even when the refractory period is very small ($\alpha\sim\pi/20$). Therefore, the weak-signaling approximation developed in this paper cannot describe a wavelength selection mechanism. This becomes even more evident as we investigate stability analysis of Eq. (36) without any assumptions on the wave speed.

V. STABILITY ANALYSIS OF THE WAVE SOLUTIONS

The reversal-point density PDE has a homogeneous solution $f\equiv N/\pi$, where N is a positive constant that represents a common value of local densities N_+ and N_- [see Eqs. (11) and (12)]. For this homogeneous solution the advection velocities in Eqs. (23) and (24) are given by

$$U\equiv 0, \quad V\equiv V_0\equiv -2(\pi-\alpha)\Omega(N). \tag{48}$$

The linearized equation for $\delta f\equiv f-N/\pi$ is

$$\partial_T\delta f + V_0\partial_t\delta f + \frac{N}{\pi}[\partial_x(\delta U)+\partial_t(\delta V)] = 2\pi(D_1+D_2)\partial_{xx}\delta f + 2\pi K\partial_{tt}\delta f. \tag{49}$$

Here, δU and δV are linearized perturbations of U and V induced by the perturbation δf of f. From Eqs. (23) and (24) we obtain

$$\delta U = \Omega'(N)\int_\alpha^\pi\int_0^\pi [\delta f(x-s+\phi,t+s+\phi) - \delta f(x+s-\phi,t+s+\phi)]d\phi ds \tag{50}$$

and

$$\delta V = -\Omega'(N)\int_\alpha^\pi\int_0^\pi [\delta f(x-s+\phi,t+s+\phi) + \delta f(x+s-\phi,t+s+\phi)]d\phi ds. \tag{51}$$

Equation (49) has exponential solutions of the form

$$\delta f(x,t,T)\propto\exp(ikx+ilt+\sigma T). \tag{52}$$

Here k is any real number and l is an integer because of the 2π periodicity of $f(x,t)$ in its second argument. The growth rate is given by

$$\Gamma\equiv \mathrm{Re}(\sigma)=\mathrm{Re}(\lambda(k,l))-2\pi(D_1+D_2)k^2-2\pi D_2 l^2, \tag{53}$$

where $\lambda(k,l)$ is defined by

$$\lambda(k,l)\delta f = -\frac{N}{\pi}[\partial_x(\delta U)+\partial_t(\delta V)], \tag{54}$$

with δf given by Eq. (52). Substituting Eq. (52) into Eq. (54) gives λ:

$$\lambda = 2i\Omega'(N)N(-1)^l\left\{e^{iK\alpha}\sin[K(\pi-\alpha)]\frac{\sin(L\pi)}{L\pi} + e^{iL\alpha}\sin[L(\pi-\alpha)]\frac{\sin(K\pi)}{K\pi}\right\}, \tag{55}$$

where

$$K\equiv\frac{l-k}{2}, \quad L\equiv\frac{l+k}{2}. \tag{56}$$

Using the result in Eq. (53) we obtain

$$\Gamma = 2\Omega'(N)N(-1)^{l+1}\left\{\sin(K\alpha)\sin[K(\pi-\alpha)]\frac{\sin(L\pi)}{L\pi} + \sin(L\alpha)\sin[L(\pi-\alpha)]\frac{\sin(K\pi)}{K\pi}\right\} - 2\pi(D_1+D_2)k^2 - 2\pi D_2 l^2. \tag{57}$$

Note that, in the limit $l\to k$, Eq. (57) reduces to the growth rate of waves with speed near 1, Eq. (45). We show that the resulting linear instability analysis does not provide a mechanism for wave speed and wave number selection.

For simplicity consider the lowest-frequency mode $l=1$ and suppose that $D_1=D_2$. Equation (57) reduces to

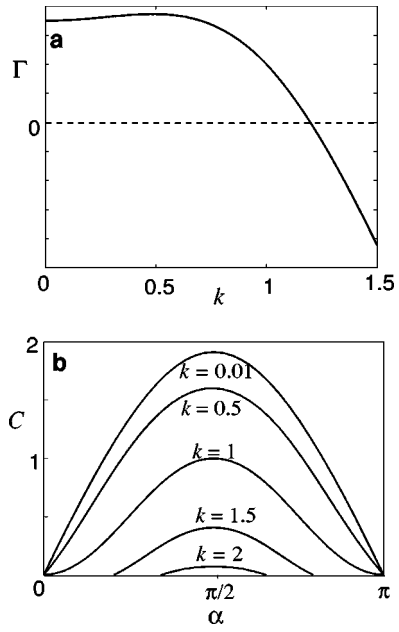

FIG. 7. (a) Growth rate Eq. (58) as a function of wave number. Parameter values $C=0.3$ and $\alpha=\pi/4$ are used. This point is denoted by an asterisk in Fig. 6. (b) Neutral stability curves for different wave numbers.

$$\Gamma = 2\Omega'(N)N\Bigg\{\sin[(1-k)\alpha/2]\sin[(1-k)(\pi-\alpha)/2] \times\frac{\sin[(1+k)\pi/2]}{(1+k)\pi/2}+\sin[(1+k)\alpha/2] \times\sin[(1+k)(\pi-\alpha)/2]\frac{\sin[(1-k)\pi/2]}{(1+k)\pi/2}-\frac{2C}{3}k^2-\frac{C}{3}\Bigg\}, \tag{58}$$

where C is defined as in Eq. (46). Figure 7(a) shows the growth rate Γ as a function of wave number k for specific values parameters C and α so that (C,α) lies in the region corresponding to growth of $k=1$ waves only (this point is denoted by an asterisk in Fig. 6). Note that the waves with wavelength (5) correspond to $k=1$ and do not have the maximum growth rate. Figure 7(b) shows neutral stability curves computed from Eq. (57) for different values of k. As one can see, the growth region for each wave number would include the growth regions of all larger wave numbers as a subset. To conclude, the results of this section show that the linear stability analysis of the weak-signaling model does not provide a wave-speed and wavelength selection mechanism. This result is corroborated by numerical solutions of the full system (1)–(4).

VI. COLLIDING WAVES

A. Reversal-point density representation of a full solution

Numerical solutions of the full system, Eqs. (1)–(4), starting from an initially random perturbation of homogeneous solution do not asymptote to periodic waves unless the signaling is sufficiently strong (data not shown). We show that

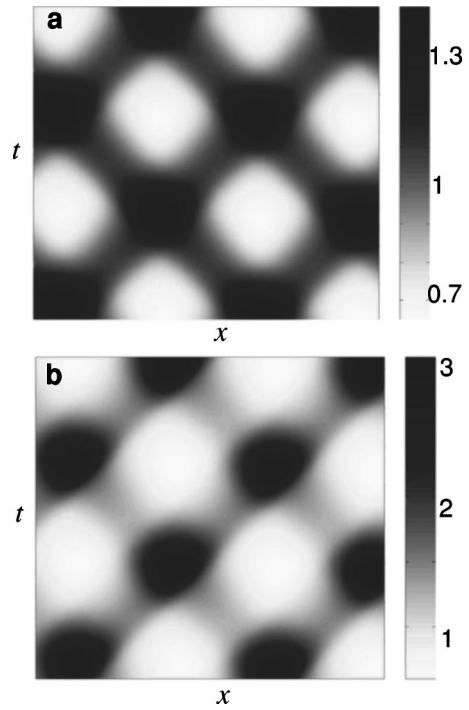

FIG. 8. (a) Space-time surface plot of the total density $N_+ + N_-$ computed from solution of the full system Eqs. (1)–(4). (b) Space-time surface plot of the reversal point density. Parameters in dimensionless units [Eq. (6)] are $\omega_1=1.2$, $D_x=D_\phi=0.01$, $\alpha=\pi/10$, and $q=4$.

the framework developed in this paper still allows us to see a focusing mechanism of the developed pattern that counteracts diffusive spreading.

At sufficiently strong signaling [$\omega_1 \gtrsim \omega_0$ in Eq. (4)], Eqs. (1)–(4) with periodic boundary conditions always asymptote to "colliding-wave" solutions: The space-time behavior of the total density $(N_+ + N_-)$ superficially resembles a superposition of counterpropagating waves with speed ±1 [Fig. 8(a)]. This pattern is often observed experimentally as a time lapse movie of consecutive phase contrast images [14,15] and experimentalists refer to "waves passing through each other without interference." That clearly distinguished these waves from developmental waves in other microorganisms such as *Dictyostelium discoideum* which are known to annihilate upon collisions [5,6]. Figure 8(a) shows a space-time plot of the total density solution. High-density bands tilted 45° and 135° from the x axis are right- and left-going crests, respectively. Figure 8(b) shows the corresponding space-time density of LR reversal points obtained from a full solution of

$$f_{LR}(x,t) \equiv n(x,\phi=0^+,t). \tag{59}$$

This equality follows from the fact that cells with the phases $0<\phi<dt$ at time t reversed during time interval $(t-dt,t)$ [see Fig. 3(a)].

Comparing Figs. 8(a) and 8(b) we conclude that most of the cells reverse during crest collisions. That means that the colliding-wave solutions of Eqs. (1)–(4) are *not* a simple superposition of two traveling waves with speeds ±1 in which the reversal-point distribution is proportional to den-

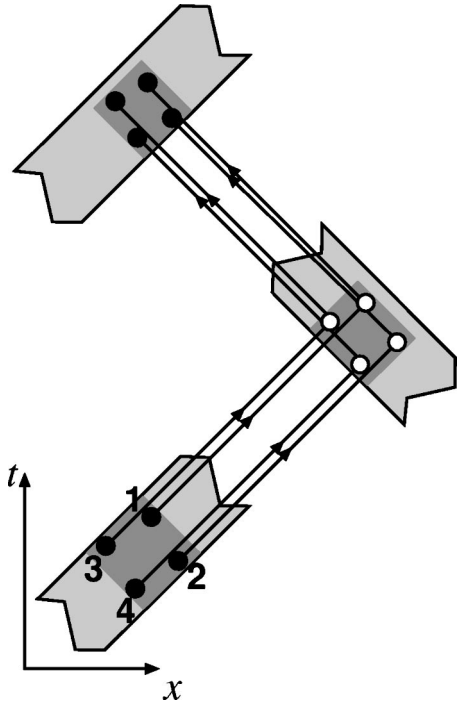

FIG. 9. Iterative focusing of colliding waves.

sity of the crest [see Eq. (13)]. Instead LR reversal points are concentrated at crest intersections. The same observation would apply if we plot the space-time density of RL reversal points $f_{RL}(x,t) \equiv n(x, \phi = \pi^+, t)$. These plots show that the traveling waves *reflect from one another on each collision;* i.e., right- and left-going crests exchange most cells. A few cells are in their refractory period during collision and do not reverse immediately. This accounts for the light bands in Fig. 8(b).

B. Focusing mechanism

The mechanism of focusing in "colliding waves" is easy to visualize by following the distribution of the reversal points (Fig. 9). Light gray bands in Fig. 9 represent dense crests [compare with Fig. 8(a)]; for simplicity, only parts of these bands are shown. Bands tilted to the right and left represent concentrations of right- and left-moving bacteria. Dark gray rectangles represent the support of reversal points. Trajectories of four sample cells are shown. As cells glide to the right they leave the concentration of left-moving cells while still refractory. The cells eventually reach the next concentration of left-moving bacteria. Since they are now sensitive, their phase clocks are accelerated. Cells in the front part of the crest (1 and 2) hit the the concentration of left-going cells before cells in the back of the crest (3 and 4). As a result they suffer more collisions so that their phase clocks are accelerated more and they reverse sooner. Thus the region of support of reversal points gets focused in the $x+t$ direction. In the same fashion cells 1 and 3 will hit the next concentration of right-moving cells before cells 2 and 4 and reverse sooner. This results in a focusing of the region in the x-t direction. Diffusional spreading would counteract the focusing to produce the final amplitude waves. The formalism developed in Sec. III makes these qualitative arguments quantitative.

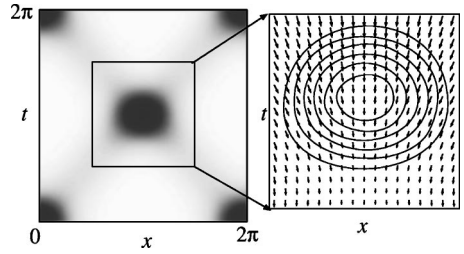

FIG. 10. Reversal-point density and convective velocity field for colliding waves. Parameters are as $\alpha = \pi/4$, $D_x = D_\phi = 0.05$, and $q = 4$.

In the weak-signaling limit the colliding waves in Fig. 8 correspond to a solution of Eq. (36) with a period near 2π in both x and t directions. Imposing these periodic boundary conditions we show that colliding waves are a stable solution of Eq. (36) but have a limited domain of attraction. Figure 10 shows a density plot of the the steady-state solution. The inset shows a contour plot of the density as well as the convective vector field (U,V). As one can see from Eq. (24), $V < 0$, and, therefore, there is a permanent downward drift of reversal points in time. This drift is nonuniform; cells drift downward faster in the upper part of the density peak of the reversal than in the lower part. Therefore, the convective velocity V focuses the peak along the time coordinate. The spatial component U of the convective velocity changes sign from positive in the left part of the peak to negative in the right part of the peak. It is zero along the symmetry axis of the peak. Thus, the velocity U results in no net drift in the spatial direction, but still produces focusing that counteracts inevitable diffusion. Since the spatial diffusion coefficient in Eq. (36) is always larger than the time diffusion, the peak spreads more in the spatial direction.

VII. SUMMARY

Pattern formation in microorganisms has been extensively studied, both experimentally and mathematically. A few notable examples include periodic patterns in colonies of *Proteus mirabilis* [24,25], *Salmonella typhimurium* [26], *Escherichia coli* [27], *Bacillus subtilis* [28], and *Dictyostelium discoideum* [3–5]. Formation of these patterns depends on diffusion-mediated chemotaxis and/or growth and death of the cells. These patterns are quite different from the rippling in myxobacteria that originates because of the synchronization of internal clocks that control the spatial motion of individual cells. The synchronization is achieved by contact-mediated signaling during end-to-end cell collisions. The existence of the refractory period is crucial for the synchronization: this is the main prediction of the model. Although refractory periods have been shown to be generic in eukaryotic systems, this is the first demonstration of a refractory period in a bacterial system [2]. The analysis performed in this work reveals the synchronization and pattern formation mechanism.

The focusing mechanism of the waves is clearly visible by tracking reversal points of cells in space-time. In the weak-signaling limit we derive an evolution equation tracing the distribution of reversal points (Sec. III). Linear stability analysis determines parameters favorable for the development of the waves with a given speed (Sec. IV), but does not reveal the wavelength and wave number selection mechanisms (Sec. V). Numerical simulations of the equations show that there are stable wave solutions corresponding to the experimentally observed ripples (Sec. VI). However, in the weak-signaling limit the basin of attraction of these patterns is small; i.e., these patterns do not develop starting from random perturbation of homogeneous initial data (Sec. VI). In fact, the numerical simulation of the full system, Eqs. (1)–(4), shows that both strong signaling and nonlinear density dependence are essential for the wave number selection mechanism. Thus, any linear stability analysis is not capable of predicting the correct wavelength. Therefore, the analysis of the wave speed and wavelength selection mechanism for the myxobacteria density waves remains an open question.

ACKNOWLEDGMENTS

The work on myxobacteria has been carried out in collaboration with the Dale Kaiser lab (Stanford University). The authors are grateful to Alex Mogilner for valuable discussions. G.O. was supported by NIH Grant No. GM59875-01A1. O.I. was supported by the Howard Hughes Medical Institute.

APPENDIX: ALTERNATIVE DERIVATION OF REVERSAL-POINT DENSITY EVOLUTION

In Sec. III we presented a geometric derivation of Eq. (36). Here we present an alternative, more formal derivation based on the asymptotic expansion of the density function $n(x,\phi,t)$. In the small-signaling and -diffusion limit [with signaling and diffusion both proportional to ϵ as in Eqs. (18) and (32)], we seek an asymptotic expansion of the density function

$$n(x,\phi,t,\epsilon) \sim n_0(x,\phi,t,\tau) + \epsilon n_1(x,\phi,t,\tau) + \cdots . \quad \text{(A1)}$$

Here τ represents the "slow time"

$$\tau \equiv \epsilon t \quad \text{(A2)}$$

and terms $n_i(x,\phi,t,\tau)$ of the perturbation series are 2π periodic in ϕ and t. The rational behind Eq. (A1) is that for $\epsilon=0$ (no signaling and no diffusion), the general solution for $n(x,\phi,t)$ is exactly 2π periodic in ϕ and t. The effect of small signaling and diffusion $(0<\epsilon\ll 1)$ is to slowly change or "modulate" the arbitrary function $f(x,t)$ which appears in Eq. (9) over a characteristic time that is $O(1/\epsilon)$. In fact, the leading-order term $n_0(x,\phi,t,\tau)$ in Eq. (A1) has the form (9) with an additional dependence upon the "slow time" τ:

$$n_0(x,\phi,t,\tau) = \begin{cases} f(x-\phi,t-\phi,\tau), & 0<\phi<\pi, \\ f(x+\phi-2\pi,t-\phi,\tau), & \pi<\phi<2\pi. \end{cases} \quad \text{(A3)}$$

The actual dependence of f upon τ is yet to be determined. The essential idea is to formulate an evolution equation f with respect to the slow time τ so that the first-order term $n_1(x,\phi,t,\tau)$ in Eq. (A1) is 2π periodic in t. The 2π periodicity of n_1 in t ensures that the perturbation ϵn_1 remains $O(\epsilon)\ll 1$ for time $t=O(1/\epsilon)$ [which correspond to $\tau=O(1)$]. Using the expansion (A1) in Eqs. (1) and (2) together with Eqs. (6), (18), and (32), it follows that the density perturbation $n_1(x,\phi,t,\tau)$ satisfies

$$\partial_t n_1 + \partial_x n_1 + \partial_\phi n_1 = \begin{cases} -\partial_\tau n_0 + D_1\partial_{xx} n_0 + D_2\partial_{\phi\phi} n_0, & \text{in } 0<\phi<\alpha, \\ -\partial_\tau n_0 - \Omega_-\partial_\phi n_0 + D_1\partial_{xx} n_0 + D_2\partial_{\phi\phi} n_0, & \text{in } \alpha<\phi<\pi, \end{cases} \quad \text{(A4)}$$

$$\partial_t n_1 - \partial_x n_1 + \partial_\phi n_1 = \begin{cases} -\partial_\tau n_0 + D_1\partial_{xx} n_0 + D_2\partial_{\phi\phi} n_0, & \text{in } \pi<\phi<\pi+\alpha, \\ -\partial_\tau n_0 - \Omega_+\partial_\phi n_0 + D_1\partial_{xx} n_0 + D_2\partial_{\phi\phi} n_0, & \text{in } \pi+\alpha<\phi<2\pi, \end{cases} \quad \text{(A5)}$$

where $\Omega_-=\Omega(N_-)$ and $\Omega_+=\Omega(N_+)$.

Boundary conditions on each of the four boundaries $\phi=0$, α, π, and $\pi+\alpha$ are required. Notice that, in the absence of diffusion, the solution of Eqs. (1) and (2) is discontinuous across these four boundaries if signaling is present, so that the flux $\omega_\pm n$ is continuous. Expanding these flux continuity conditions in the limit of small signaling one obtains conditions for n_0 and n_1. The zero-order condition requires continuity of n_0 and it is satisfied by the solution, Eq. (A3). The first-order-in-ϵ term allows us to compute the jumps of n_1 across the phase boundaries:

$$[n_1]_{\phi=0} \equiv n_1\big|_{\phi=0^+} - n_1\big|_{\phi=2\pi} = \Omega_+ n_0\big|_{\phi=2\pi}, \quad \text{(A6)}$$

$$[n_1]_{\phi=0} \equiv n_1\big|_{\phi=\alpha^+} - n_1\big|_{\phi=\alpha^-} = -\Omega_- n_0\big|_{\phi=\alpha}, \quad \text{(A7)}$$

$$[n_1]_{\phi=\pi} \equiv n_1\big|_{\phi=\pi^+} - n_1\big|_{\phi=\pi^-} = \Omega_- n_0\big|_{\phi=\pi}, \quad \text{(A8)}$$

$$[n_1]_{\phi=\pi+\alpha} \equiv n_1\big|_{\phi=\pi+\alpha^+} - n_1\big|_{\pi+\alpha^-} = -\Omega_+ n_0\big|_{\phi=\pi+\alpha}. \quad \text{(A9)}$$

For small phase diffusion $D_2>0$, the density n is actually continuous across the four phase boundaries but there are sharp boundary layers of thickness $O(\epsilon)$ about the boundary points $\phi=0$, α, π, and $\pi+\alpha$. The jumps across these boundary layers are, to leading order in ϵ, the same as in the case of zero phase diffusion.

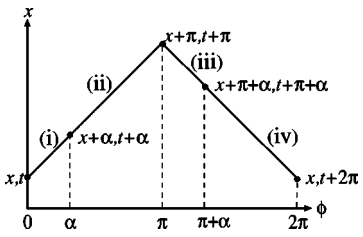

FIG. 11. Characteristics of Eqs. (A4) and (A5) projected onto the x,ϕ plane.

Figure 11 shows characteristics of the left-hand side of Eqs. (A4) and (A5) projected onto the x,ϕ plane. The changes $\delta n_1^{(\mathrm{i})\text{-}(\mathrm{iv})}$ of density n_1 along each of the segments (i)–(iv) (Fig. 11) are straightforward to compute integrating the right-hand sides of Eqs. (A4) and (A5) with use of Eq. (A3):

$$\delta n_1^{(\mathrm{i})} = \alpha[-\partial_\tau + D_1\partial_{xx} + D_2(\partial_t + \partial_x)^2]f, \tag{A10}$$

$$\delta n_1^{(\mathrm{ii})} = (\pi - \alpha)[-\partial_\tau + D_1\partial_{xx} + D_2(\partial_t + \partial_x)^2]f + (\partial_t + \partial_x)f\int_\alpha^\pi \Omega_-(x+s,t+s)ds, \tag{A11}$$

$$\delta n_1^{(\mathrm{iii})} = \alpha[-\partial_\tau + D_1\partial_{xx} + D_2(\partial_t - \partial_x)^2]f, \tag{A12}$$

$$\delta n_1^{(\mathrm{iv})} = (\pi - \alpha)[-\partial_\tau + D_1\partial_{xx} + D_2(\partial_t - \partial_x)^2]f + (\partial_t - \partial_x)f\int_{\pi+\alpha}^{2\pi} \Omega_-(x+s,t+s)ds. \tag{A13}$$

Enforcing 2π periodicity in t, one computes the change in n_1 along the characteristic line shown in Fig. 11 from x,t to $x,t+2\pi$ as

$$n_1\big|_{\phi=2\pi} - n_1\big|_{\phi=0^+} = -[n_1]_{\phi=0} = \delta n_1^{(\mathrm{i})} + [n_1]_{\phi=\alpha} + \delta n_1^{(\mathrm{ii})} + [n_1]_{\phi=\pi} + \delta n_1^{(\mathrm{iii})} + [n_1]_{\phi=\pi+\alpha} + \delta n_1^{(\mathrm{iv})}. \tag{A14}$$

Using Eqs. (A3) and (A6)–(A13) in Eq. (A14), after cumbersome but straightforward calculations, one obtains the following equation for $f(x,t,\tau)$:

$$\partial_\tau f + \frac{1}{2\pi}[\partial_x(Uf) + \partial_t(Vf)] = (D_1 + D_2)\partial_{xx}f + D_2\partial_{tt}f, \tag{A15}$$

where U and V are defined by Eqs. (20) and (22) or, equivalently, by Eqs. (23) and (24). This equation is equivalent to Eq. (36) since $\tau = 2\pi T$.

[1] A. Cheer, J.-P. Vincent, R. Nuccitelli, and G. Oster, J. Theor. Biol. **124**, 377 (1987).
[2] J. D. Murray, *Mathematical Biology*, 3rd ed. (Springer, New York, 2002).
[3] T. Hofer, J. Sherratt, and P. Maini, Proc. R. Soc. London, Ser. B **259**, 249 (1995).
[4] J. J. Tyson and J. D. Murray, Development **106**, 421 (1989).
[5] F. Siegert and C. Weijer, Curr. Biol. **5**, 937 (1995).
[6] E. Palsson and E. C. Cox, Proc. Natl. Acad. Sci. U.S.A. **93**, 1151 (1996).
[7] H. Meinhardt, P. Prusinkiewicz, and D. Fowler, *The Algorithmic Beauty of Sea Shells*, The Virtual Laboratory, 2nd ed. (Springer, Berlin, 1998).
[8] J. Campbell, B. Ermentrout, and G. Oster, Veliger **28**, 369 (1986).
[9] J. D. Murray and M. R. Myerscough, J. Theor. Biol. **149**, 339 (1991).
[10] J. D. Murray, Philos. Trans. R. Soc. London, Ser. B **295**, 473 (1981).
[11] M. Dworkin and D. Kaiser, *Myxobacteria II* (American Society for Microbiology, Washington, D.C., 1993).
[12] D. Kaiser, Nat. Rev. Microbiol. **1**, 45 (2003).
[13] B. Sager and D. Kaiser, Genes Dev. **7**, 1645 (1993).
[14] B. Sager and D. Kaiser, Genes Dev. **8**, 2793 (1994).
[15] R. Welch and D. Kaiser, Proc. Natl. Acad. Sci. U.S.A. **98**, 14 907 (2001).
[16] L. Jelsbak and L. Sogaard-Andersen, Curr. Opin. Microbiol. **3**, 637 (2000).
[17] H. Kuhlwein and H. Reichenbach (unpublished).
[18] H. Reichenbach, Ber. Dtsch. Bot. Ges. **78**, 102 (1965).
[19] A. Winfree, *The Geometry of Biological Time*, 2nd ed. (Springer-Verlag, Berlin, 2001).
[20] M. Dworkin and D. Eide, J. Bacteriol. **154**, 437 (1983).
[21] D. Kaiser, Curr. Opin. Microbiol. **1**, 663 (1998).
[22] O. A. Igoshin, A. Mogilner, R. Welch, D. Kaiser, and G. Oster, Proc. Natl. Acad. Sci. U.S.A. **98**, 14 913 (2001).
[23] O. A. Igoshin, R. Welch, D. Kaiser, and G. Oster, Proc. Natl. Acad. Sci. U.S.A. **101**, 4256 (2004).
[24] S. Esipov and J. Shapiro, J. Math. Biol. **36**, 249 (1997).
[25] A. Czirok, M. Matsushita, and T. Vicsek, Phys. Rev. E **63**, 031915 (2001).
[26] D. E. Woodward, R. Tyson, M. R. Myerscough, J. D. Murray, E. O. Budrene, and H. C. Berg, Biophys. J. **68**, 2181 (1995).
[27] R. Tyson, S. R. Lubkin, and J. D. Murray, Proc. R. Soc. London, Ser. B **266**, 299 (1999).
[28] N. Mendelson and J. Lega, J. Bacteriol. **180**, 3285 (1998).